Stepwise Evolution of Spherical Seeds into 20-Fold Twinned Icosahedra

Mark R. Langille *et al.*

Science **337**, 954 (2012);
DOI: 10.1126/science.1225653

Fig. 2A. With Ti present, the system adopts a complex alloy configuration where Ti and W are heterogeneously distributed on the nanoscale as a polycrystalline body-centered cubic (BCC) structure, with no signatures of any amorphous content. This heterogeneous distribution is illustrated by the chemical arrangement in the equilibrated alloy in Fig. 3, with Fig. 3A showing the atomic contrast between W and Ti and Fig. 3B showing a local chemical map based on energy dispersive spectroscopy (*35*). A compositional line scan in Fig. 3C reveals the magnitude of the Ti composition ranging from near 0 atomic % to about 50 atomic %.

The nanoscale chemical distribution seen in Fig. 3 is not expected for a bulk equilibrium alloy, where Ti is soluble to 48 atomic % in W at the equilibration temperature, and a homogeneous chemical distribution should be observed. This solute distribution is a consequence of the nanostructure: The high volume fraction of grain boundaries creates different chemical configurations, and a lower energy state results from the heterogeneous solute distribution. In a nanoscale structure, a heterogeneous solute distribution is explicitly expected from Eq. 2.

From a technological standpoint, the results in Figs. 2 and 3 suggest that nanocrystalline tungsten can, in principle, be made sufficiently stable to survive a typical consolidation thermal cycle. Given the exceptionally high strength of nanocrystalline BCC metals (*37*) and the unusual secondary properties (such as shear localization) that emerge at these grain sizes, the present results may speak to a new family of engineering tungsten alloys. At the same time, our experimental work on W-Ti is simply an example of a single alloy design exercise; the above approach may be applied again to a number of different base metals.

References and Notes

1. K. Lu, L. Lu, S. Suresh, *Science* **324**, 349 (2009).
2. J. R. Weertman *et al.*, *MRS Bull.* **24**, 44 (1999).
3. H. Van Swygenhoven, J. R. Weertman, *Mater. Today* **9**, 24 (2006).
4. X. Z. Liao, F. Zhou, E. J. Lavernia, D. W. He, Y. T. Zhu, *Appl. Phys. Lett.* **83**, 5062 (2003).
5. L. Lu, M. L. Sui, K. Lu, *Science* **287**, 1463 (2000).
6. L. Lu, Y. Shen, X. Chen, L. Qian, K. Lu, *Science* **304**, 422 (2004).
7. Y. Wang, M. Chen, F. Zhou, E. Ma, *Nature* **419**, 912 (2002).
8. D. B. Witkin, E. J. Lavernia, *Prog. Mater. Sci.* **51**, 1 (2006).
9. B. Poudel *et al.*, *Science* **320**, 634 (2008).
10. M. E. McHenry, M. A. Willard, D. E. Laughlin, *Prog. Mater. Sci.* **44**, 291 (1999).
11. M. Ames *et al.*, *Acta Mater.* **56**, 4255 (2008).
12. J. Weissmüller, *Nanostructured Mater.* **3**, 261 (1993).
13. R. Kirchheim, *Acta Mater.* **50**, 413 (2002).
14. R. Kirchheim, *Acta Mater.* **55**, 5129 (2007).
15. R. Kirchheim, *Acta Mater.* **55**, 5139 (2007).
16. P. C. Millett, R. P. Selvam, A. Saxena, *Acta Mater.* **55**, 2329 (2007).
17. J. Luo, H. Cheng, K. M. Asl, C. J. Kiely, M. P. Harmer, *Science* **333**, 1730 (2011).
18. M. Baram, D. Chatain, W. D. Kaplan, *Science* **332**, 206 (2011).
19. M. Kahlweit, *Science* **240**, 617 (1988).
20. A. J. Detor, C. A. Schuh, *Acta Mater.* **55**, 4221 (2007).
21. A. J. Detor, C. A. Schuh, *J. Mater. Res.* **22**, 3233 (2007).
22. T. Hentschel, D. Isheim, R. Kirchheim, F. Muller, H. Kreye, *Acta Mater.* **48**, 933 (2000).
23. P. Choi, M. da Silva, U. Klement, T. Al-Kassab, R. Kirchheim, *Acta Mater.* **53**, 4473 (2005).
24. K. A. Darling, B. K. VanLeeuwen, C. C. Koch, R. O. Scattergood, *Mater. Sci. Eng. A* **527**, 3572 (2010).
25. F. Liu, R. Kirchheim, *Scr. Mater.* **51**, 521 (2004).
26. C. E. Krill, H. Ehrhardt, R. Birringer, *Z. Metallk.* **96**, 1134 (2005).
27. S. G. Mayr, D. Bedorf, *Phys. Rev. B* **76**, 024111 (2007).
28. C. Koch, R. Scattergood, K. Darling, J. Semones, *J. Mater. Sci.* **43**, 7264 (2008).
29. J. R. Trelewicz, C. A. Schuh, *Phys. Rev. B* **79**, 094112 (2009).
30. D. Roundy, C. R. Krenn, M. L. Cohen, J. W. Morris Jr., *Philos. Mag. A* **81**, 1725 (2001).
31. Q. Wei *et al.*, *Appl. Phys. Lett.* **86**, 101907 (2005).
32. L. J. Kecskes *et al.*, *Mater. Sci. Eng. A* **467**, 33 (2007).
33. H. W. Hayden, J. H. Brophy, *J. Electrochem. Soc.* **110**, 805 (1963).
34. R. M. German, Z. A. Munir, *Metall. Trans. A* **7**, 1873 (1976).
35. Materials and methods are available as supplementary materials on *Science* Online.
36. S. Jonsson, *Z. Metallk.* **87**, 784 (1996).
37. C. R. Krenn, D. Roundy, J. W. Morris Jr., M. L. Cohen, *Mater. Sci. Eng. A* **319–321**, 111 (2001).

Acknowledgments: This work was supported by the U.S. Army Research Office under grant no. W911NF-09-1-0422. MIT has applied for a patent, application no. PCT/US12/28811, related to the design methods and materials produced in this work. Additional information and data used in this work can be found in the supplementary materials.

Supplementary Materials

www.sciencemag.org/cgi/content/full/337/6097/951/DC1
Materials and Methods
Figs. S1 and S2
Tables S1 and S2
References (*38–50*)

15 May 2012; accepted 13 July 2012
10.1126/science.1224737

Stepwise Evolution of Spherical Seeds into 20-Fold Twinned Icosahedra

Mark R. Langille,[1] Jian Zhang,[1] Michelle L. Personick,[1] Shuyou Li,[2] Chad A. Mirkin[1,2]*

Understanding the factors that influence the growth and final shape of noble metal nanostructures is important for controlling their properties. However, relative to their single-crystalline counterparts, the growth of nanoparticles that contain twin defects can be difficult to control because multiple competitive growth pathways can yield such structures. We used spherical, cubic, and octahedral single-crystalline gold nanoparticles as dual electron microscopy labels and plasmonic seeds to track the growth of multiply twinned silver nanostructures. As the bimetallic nanostructures grew, they successively developed twin planes to ultimately form multiply twinned nanoparticles from single-crystalline seeds. Collectively, these data demonstrate how a series of nanoparticles of different shapes and internal crystal structures are interrelated and develop from one another.

Complicated reaction pathways and transformations can be studied in molecular materials by distinctly labeling starting materials and monitoring their evolution over time with techniques such as fluorescence and isotopic labeling. A comparable strategy for monitoring nanoparticle growth is to use a nanoparticle of one material (e.g., Au) as both a seed and an electron microscopy label to follow the growth of a second material type (e.g., Ag). (*1*) This method has provided insight into the role of particular reaction conditions in controlling nanoparticle growth (*1*, *2*). In the synthesis of noble metal nanoparticles, there is often a wide variety of conditions that can lead to different growth processes and create markedly different nanoparticle shapes (*3*). We report a method for following the growth of a nanoparticle from a single-crystalline, pseudo-spherical Au seed into a bimetallic Ag-Au icosahedron structure. We have identified eight intermediate structures formed along the way, as well as some of the key factors that control each of the stepwise growth processes.

In the case of defect-free or single-crystalline noble metal nanoparticles, shape control can be achieved by directing the deposition preference onto specific crystallographic facets through the use of additives or capping agents (*3–8*). However, nanoparticle growth can be more difficult to control when multiply twinned structures such as decahedra and icosahedra are involved because these structures can grow from multiple competitive growth pathways (*3*, *9–12*). Unlike their single-crystalline counterparts, twinned particles can grow from either twinned or single-crystalline seeds. One pathway involves the nucleation of a twinned nanoparticle seed and its subsequent growth in a layer-by-layer fashion (*13*). Alternatively, a single-crystalline nanoparticle seed can develop twin defects during its growth (or through a coalescence/fusion mechanism) to yield a twinned structure (*14*, *15*). Understanding from which of these pathways twinned nanoparticles develop is important for controlling reaction conditions so as to selectively enhance or suppress their growth.

Electron microscopy provides a way of monitoring certain aspects of particle growth,

[1]Department of Chemistry and International Institute for Nanotechnology, Northwestern University, Evanston, IL 60208, USA. [2]Department of Materials Science and Engineering, Northwestern University, Evanston, IL 60208, USA.

*To whom correspondence should be addressed. E-mail: chadnano@northwestern.edu

and a number of studies have even been able to track individual nanoparticle growth in real time (*14*, *16*–*18*). However, studies to date typically do not allow one to track what is happening to individual particles as a function of growth conditions (*19*), or if they do, the solution conditions in which they can be studied are quite limited (*14*, *16*–*18*).

In prior work (*1*), we showed that gold nanoparticles can be used as plasmonic seeds to grow silver shells and ultimately form bimetallic triangular prisms in a plasmon-mediated synthesis (*20*–*23*). In the transmission electron microscopy (TEM) images of such structures, we differentiated the spherical gold cores from the triangular prism silver shells according to their difference in electron-scattering efficiencies. We hypothesized that such plasmonic labels would be ideal for monitoring the stepwise transformation of gold nanoparticle seeds into a series of more complicated bimetallic nanoparticles that differ in shape and internal structure. In a typical experiment, pseudo-spherical Au nanoparticles (diameter ~25 nm) were used as dual plasmonic seeds and TEM labels (Fig. 1A) to grow bimetallic nanoparticles with Au cores and Ag shells. A growth solution was prepared by adding $AgNO_3$, sodium citrate, bis-(*p*-sulfonatophenyl)-phenylphosphine dihydrate potassium salt (BSPP), and an aliquot of the Au seeds to an aqueous solution. The light-induced reaction was initiated by irradiating the growth solution for 12 hours with a 150-W halogen lamp using a bandpass filter centered at 550 ± 20 nm, commensurate with the optical absorbance of the seed particles (*22*, *24*).

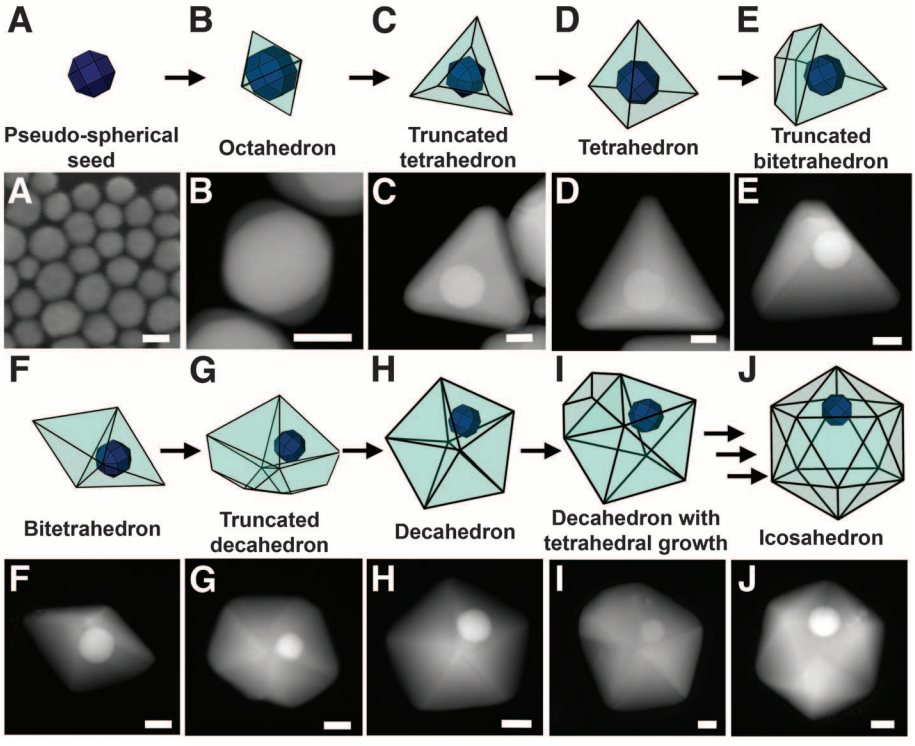

Fig. 1. Models and representative STEM images depicting the proposed growth pathway of a single-crystalline seed in this plasmon-mediated reaction. (**A**) STEM image of the pseudo-spherical single-crystalline Au seeds. (**B** to **J**) STEM images of bimetallic particles with (B) octahedral, (C) truncated tetrahedral, (D) tetrahedral, (E) truncated bitetrahedral, (F) bitetrahedral, (G) truncated decahedral, (H) decahedral, (I) decahedral with an additional tetrahedral growth, and (J) icosahedral morphologies, which were all observed as products of the same reaction. Scale bars, 25 nm. See fig. S7 for models of a more detailed growth scheme from (I) to (J) (*24*).

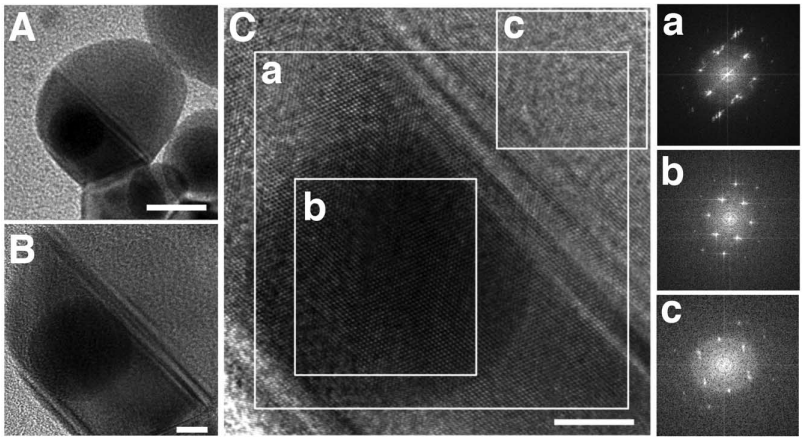

Fig. 2. (**A** and **B**) High-magnification TEM (A) and HRTEM (B) images of a truncated bitetrahedron. Scale bars, 20 nm (A), 5 nm (B). (**C**) Fourier transform (FT) of each of the regions (**a** to **c**) indicated in the HRTEM image on the left. Scale bar, 5 nm. Region a encompasses all sections of the particle and exhibits multiple sets of spots, indicating the existence of multiple crystals. Region b is a FT of the Au seed and shows a single set of spots, confirming that the seed is single-crystalline. Region c is on the opposite side of the twin plane from the gold seed, and thus has a different FT pattern.

Characterization of the reaction products by scanning transmission electron microscopy (STEM) showed that a variety of different nanoparticle shapes were produced in the same reaction, such as bitetrahedra, decahedra, and icosahedra (Fig. 1 and fig. S1) (*24*). These particular {111}-faceted particle shapes are all related in that they consist of 2, 5, and 20 tetrahedral subunits, respectively, separated by twin boundaries (*10*). Note that the presence of twin planes is assumed on the basis of particle shape and confirmed by high-resolution TEM (HRTEM) (figs. S2 and S3) (*10*, *24*). In each particle, an Au nanoparticle label appears in brighter contrast than the surrounding Ag shell. This interpretation of the STEM contrast was confirmed by energy-dispersive x-ray spectroscopy (EDX; fig. S4) (*24*). In all cases, the Au nanoparticle labels were located within a single tetrahedral subunit of each structure (figs. S5 and S6) (*24*). These data reveal that all of the observed particle shapes can indeed grow from a single-crystalline nanoparticle seed (Fig. 2 and fig. S2) and show that in this synthetic system, multiply twinned particles grow by a process of successive twinning (*24*). However, the relation between these different bimetallic products remains unclear in this experiment.

To probe suspected shape transformations that occur as a single-crystalline seed develops into an icosahedron, we studied the effects of initiating the reaction with gold seeds having well-defined shapes. Because all of the particles produced in this reaction were bound by {111} surface faces, we chose to study the growth process starting with cubic Au seeds (edge length ~50 nm) that are bound by {100} surface facets (fig. S8A) (*24*). In this way, we studied the transformation of such seeds into {111}-faceted structures. In a typical experiment, a solution of the cubes was irradiated at 550 nm (a wavelength that excited the dipole plasmon resonance of the cubes) and

Ag from the growth solution was then deposited onto the seed structures. These conditions are identical to those used for the pseudo-spherical seeds described above, which are bound by a mixture of {111}, {100}, and/or {110} facets (*3*). The majority of the structures produced from the well-defined Au cubic seeds were bimetallic octahedra, as confirmed by TEM and EDX (Fig. 3). The shape transformation of an Au cube into a bimetallic octahedron occurred by the preferential deposition of Ag onto the {100} facets of the cube until the structure was fully transformed into a {111}-faceted octahedron. In the case of the pseudo-spherical seeds, octahedra also formed, but the bimetallic structures observed (Fig. 1B) were smaller than those produced from the gold cubes. Indeed, the size of the seed dictated the size of the resulting octahedron; the reason for this observation is that the transformation of seeds with less stable surface facets into octahedra with more stable {111} surface facets was rapid relative to further growth of octahedra into larger octahedral structures. Thus, the initial silver ions in the reaction were rapidly consumed to effect the seed-to-octahedron transformation. We observed some particles with Au cubic cores and both truncated and fully developed tetrahedral Ag shells (fig. S9), indicating that these structures underwent additional shape transformations after developing into octahedra, analogous to the particle shapes observed in Fig. 1, C and D (*24*). This data set provides a way of studying the first steps in Fig. 1 (A-to-B, A-to-C, and A-to-D) by starting from a seed with relatively well-defined surface facets.

To further study the subsequent growth steps in the transformation of pseudo-spherical seeds into icosahedra, we synthesized Au octahedra (edge length ~50 nm; fig. S8B) and used them as plasmonic seeds to grow bimetallic structures under the same experimental conditions as described above (*24*). The majority of the structures produced from the Au octahedral seeds were either truncated or fully developed bimetallic tetrahedra (Fig. 4), consistent with the B-to-C-to-D transformation in Fig. 1. EDX was again used to confirm the metallic distribution of these nanoparticles with Au cores and Ag shells (Fig. 4, E to G).

The shape transformation of a {111}-faceted octahedron into a {111}-faceted tetrahedron was unexpected because it requires the asymmetric growth of the octahedron while maintaining the same surface facets. Additionally, the growth of fully developed tetrahedra is atypical because both fully developed and corner-truncated tetrahedra expose {111} surface facets, which provides little driving force for the growth of the fourth tip (*25*, *26*). We hypothesized that the formation of the tetrahedra was a result of twinning, which is often a consequence of plasmon-mediated syntheses (*20*, *21*, *27*, *28*). We propose that as an octahedron grows in size, a twin plane develops along one of its {111} faces. Twin defects contain self-propagating ledges that serve as active sites for crystal growth, and Ag deposition along the {111} plane of the twin defect is faster than along the other {111} faces (*3*). This event results in asymmetric nanoparticle growth and drives the transformation from octahedron to truncated tetrahedron. This observation is consistent with previous studies in which, in the absence of Au seeds, planar twinned {111}-faceted triangular prisms are formed under otherwise similar conditions (*27*).

It has been observed experimentally (*29*, *30*) and also suggested by theoretical calculations (*31*) that small metal clusters can undergo structure fluctuations in which the twinning motif can change to lower the overall energy of the nanoparticle. However, researchers have concluded that as a cluster grows, it will reach a size threshold at which the energy barrier for structural change becomes too great (*29*–*31*). The growth of a single stable twin plane can induce the growth of additional twin planes such that either a five-fold (decahedral) or 20-fold (icosahedral) twinning motif is adopted (*31*). A similar process was observed in this plasmon-mediated reaction, where the growth of a single twin defect in an octahedral particle not only effected the transformation from

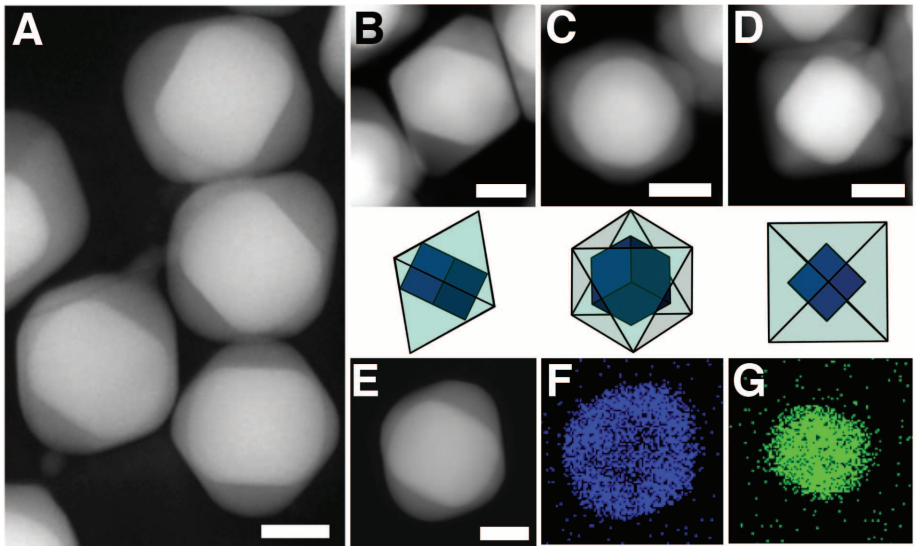

Fig. 3. Products generated when the reaction is seeded with Au cubes. (**A**) Typical STEM image of nanoparticles with Au cube core and Ag octahedron shell. (**B** to **D**) Heterometallic octahedra and their corresponding models, viewed at different orientations with respect to the electron beam and approximately aligned to the [110] (B), [111] (C), and [100] (D) zone axis. (**E**) STEM image of an individual particle. (**F** and **G**) EDX maps of the Ag components (F) and the Au components (G) of the particle in (E). Scale bars, 25 nm.

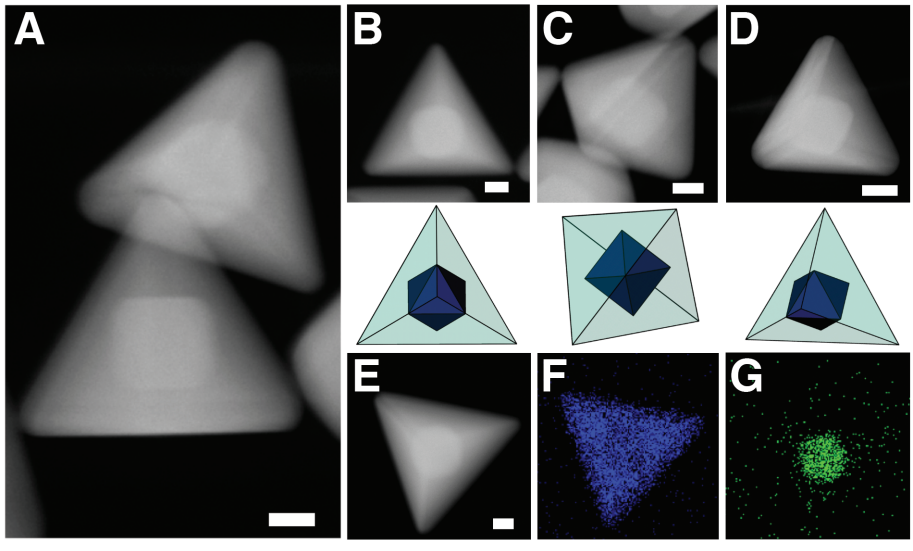

Fig. 4. Products generated when the reaction is seeded with Au octahedra. (**A**) Typical STEM image of nanoparticles with Au octahedron core and Ag tetrahedron shell. (**B** to **D**) Heterometallic tetrahedra and their corresponding models, viewed at different orientations to the electron beam and approximately aligned to the [111] (B), [100] (C), and slightly tilted from the [111] (D) zone axis. (**E**) STEM image of an individual particle. (**F** and **G**) EDX maps of the Ag components (F) and the Au components (G) of the particle in (E). Scale bars, 25 nm.

octahedron to truncated tetrahedron, but also induced the growth of a second twin boundary along a neighboring {111} face that is about 72° apart from the first (*10*). Thus, the driving force for the growth of the fourth tip of the tetrahedron is likely rapid growth along two adjacent twin boundaries (Fig. 1D). This conclusion is supported by high-magnification STEM images of individual, fully formed tetrahedra that show distinct lines of contrast along their edges, suggesting the presence of twin planes running parallel to the faces of the tetrahedra, and was further confirmed by electron diffraction studies (figs. S10 to S12) (*24*).

Later stages of the growth pathway outlined in Fig. 1 were probed by increasing the silver/gold ratio in the reaction seeded with Au octahedra. When the number of Au octahedral seeds added to the reaction was reduced (effectively increasing the silver/gold ratio), bimetallic particles with truncated bitetrahedral and even decahedral Ag shells formed (fig. S13). We observed a large dispersity in terms of particle shape in this reaction, similar to what occurred when we used pseudo-spherical seeds. These data indicate that tetrahedra continued to develop twin defects such that a five-fold twinned decahedron could form. STEM images from the growth of the pseudo-spherical seeds revealed bimetallic particles with truncated bitetrahedral, bitetrahedral, truncated decahedral, and decahedral shapes (Fig. 1, E to H). We propose that a tetrahedron can develop a third twin plane, causing a change in shape to a bitetrahedron, and then eventually develop a fourth and fifth twin plane, resulting in the growth of a decahedron.

The lack of synthetic procedures for preparing Au analogs for many of the shapes depicted in Fig. 1, C to G, prevented a closer study of these individual growth steps. However, we have previously studied the plasmon-mediated deposition of Ag onto Au decahedral seeds under nearly identical conditions (*2*). We found that Au five-fold twinned decahedra grew into bimetallic 20-fold twinned icosahedra in a manner similar to the transformations outlined in Fig. 1. These data are consistent with the conclusion that, for this synthetic system, multiply twinned particles formed by successive twinning and that decahedra, regardless of whether they comprise Au or Au-core/Ag-shell structures, can transform into icosahedra through this twinning process (Fig. 1, H to J).

These data show that this particle labeling strategy is particularly useful for elucidating growth pathways when crystal twinning is involved. This method of analysis allows for the discrimination of twin defects inherent to the seed particle and those that develop during the growth of a crystal, essentially distinguishing the potential growth pathways of multiply twinned nanoparticles. This work not only provides valuable insight into the growth mechanisms of multiply twinned structures, which will help to more effectively synthesize such particles in the future, but also demonstrates how nanoparticle labels can be used to effectively track and monitor the growth of nanomaterials in much the same manner that fluorescence and isotopic labeling strategies have been used to study molecular materials. We also anticipate that if this method of analysis is combined with in situ TEM observations (*14*, *16*–*18*), an even greater understanding of nanoparticle growth can be obtained.

References and Notes

1. C. Xue, J. E. Millstone, S. Li, C. A. Mirkin, *Angew. Chem. Int. Ed.* **46**, 8436 (2007).
2. M. R. Langille, J. Zhang, C. A. Mirkin, *Angew. Chem. Int. Ed.* **50**, 3543 (2011).
3. Y. Xia, Y. Xiong, B. Lim, S. E. Skrabalak, *Angew. Chem. Int. Ed.* **48**, 60 (2009).
4. W. Niu *et al.*, *J. Am. Chem. Soc.* **131**, 697 (2009).
5. J. Zeng *et al.*, *J. Am. Chem. Soc.* **132**, 8552 (2010).
6. M. L. Personick, M. R. Langille, J. Zhang, C. A. Mirkin, *Nano Lett.* **11**, 3394 (2011).
7. T. K. Sau, C. J. Murphy, *J. Am. Chem. Soc.* **126**, 8648 (2004).
8. B. Nikoobakht, M. A. El-Sayed, *Chem. Mater.* **15**, 1957 (2003).
9. W. Niu, G. Xu, *Nano Today* **6**, 265 (2011).
10. H. Hofmeister, *Z. Kristallogr.* **224**, 528 (2009).
11. Q. Zhang, J. Xie, Y. Yu, J. Yang, J. Y. Lee, *Small* **6**, 523 (2010).
12. B. Wiley, T. Herricks, Y. Sun, Y. Xia, *Nano Lett.* **4**, 1733 (2004).
13. J. G. Allpress, J. V. Sanders, *Surf. Sci.* **7**, 1 (1967).
14. K. Yagi, K. Takayanagi, K. Kobayashi, G. Honjo, *J. Cryst. Growth* **28**, 117 (1975).
15. H. Hofmeister, *Thin Solid Films* **116**, 151 (1984).
16. N. de Jonge, F. M. Ross, *Nat. Nanotechnol.* **6**, 695 (2011).
17. H. Zheng *et al.*, *Science* **324**, 1309 (2009).
18. J. M. Yuk *et al.*, *Science* **336**, 61 (2012).
19. M. Tsuji *et al.*, *Cryst. Growth Des.* **10**, 296 (2010).
20. R. Jin *et al.*, *Science* **294**, 1901 (2001).
21. R. Jin *et al.*, *Nature* **425**, 487 (2003).
22. C. Xue, G. S. Métraux, J. E. Millstone, C. A. Mirkin, *J. Am. Chem. Soc.* **130**, 8337 (2008).
23. X. Wu *et al.*, *J. Am. Chem. Soc.* **130**, 9500 (2008).
24. See supplementary materials on *Science* Online.
25. F. Kim, S. Connor, H. Song, T. Kuykendall, P. Yang, *Angew. Chem. Int. Ed.* **43**, 3673 (2004).
26. J. Zhou *et al.*, *Langmuir* **24**, 10407 (2008).
27. J. Zhang, M. R. Langille, C. A. Mirkin, *J. Am. Chem. Soc.* **132**, 12502 (2010).
28. B. Pietrobon, V. Kitaev, *Chem. Mater.* **20**, 5186 (2008).
29. J. L. Elechiguerra, J. Reyes-Gasga, M. J. Yacamán, *J. Mater. Chem.* **16**, 3906 (2006).
30. D. J. Smith, A. K. Petford-Long, L. R. Wallenberg, J.-O. Bovin, *Science* **233**, 872 (1986).
31. F. Baletto, R. Ferrando, *Rev. Mod. Phys.* **77**, 371 (2005).

Acknowledgments: This material is based on work supported by the U.S. Air Force Office of Scientific Research; the U.S. Department of Defense National Security Science and Engineering Faculty Fellowships Program/Naval Postgraduate School (award N00244-09-1-0012); the Non-equilibrium Energy Research Center, an Energy Frontier Research Center funded by the U.S. Department of Energy, Office of Science, Office of Basic Energy Sciences under award DE-SC0000989; and the NSF Materials Research Science and Engineering Center (MRSEC) program (DMR-1121262) at the Materials Research Center of Northwestern University. The microscopy work was performed in the EPIC facility of the NUANCE Center at Northwestern University, which is supported by NSF Nanoscale Science and Engineering Center, NSF MRSEC, the Keck Foundation, the State of Illinois, and Northwestern University. This work was also supported by the U.S. Air Force Office of Scientific Research through National Defense Science and Engineering graduate fellowship 32 CFR 168a (M.L.P.). Any opinions, findings, and conclusions or recommendations expressed in this publication are those of the authors and do not necessarily reflect the views of the agency sponsors.

Supplementary Materials

www.sciencemag.org/cgi/content/full/337/6097/954/DC1
Materials and Methods
Figs. S1 to S13
References (*32*, *33*)

5 June 2012; accepted 10 July 2012
10.1126/science.1225653

Mapping the Origins and Expansion of the Indo-European Language Family

Remco Bouckaert,[1] Philippe Lemey,[2] Michael Dunn,[3,4] Simon J. Greenhill,[5,6] Alexander V. Alekseyenko,[7] Alexei J. Drummond,[1,8] Russell D. Gray,[5,9] Marc A. Suchard,[10,11,12] Quentin D. Atkinson[5,13]*

There are two competing hypotheses for the origin of the Indo-European language family. The conventional view places the homeland in the Pontic steppes about 6000 years ago. An alternative hypothesis claims that the languages spread from Anatolia with the expansion of farming 8000 to 9500 years ago. We used Bayesian phylogeographic approaches, together with basic vocabulary data from 103 ancient and contemporary Indo-European languages, to explicitly model the expansion of the family and test these hypotheses. We found decisive support for an Anatolian origin over a steppe origin. Both the inferred timing and root location of the Indo-European language trees fit with an agricultural expansion from Anatolia beginning 8000 to 9500 years ago. These results highlight the critical role that phylogeographic inference can play in resolving debates about human prehistory.

Model-based methods for Bayesian inference of phylogeny have been applied to comparative basic vocabulary data to infer ancestral relationships between languages (*1*–*3*). Such studies have focused on the use of subgrouping and time-depth estimates to test competing hypotheses, but they lack explicit geographic models of language expansion. Here, we used two novel quantitative phylogeographic inference tools derived from stochastic models in evolutionary biology to tackle the "most recalcitrant problem in historical linguistics" (*4*)—the origin of the Indo-European languages. The "steppe hypothesis" posits an origin in the Pontic steppe region north of the Caspian Sea. Although the archaeological record provides a number of candidate expansions from this area (*5*), a steppe homeland is most commonly linked to evidence